Supplementary Information

Simple fluorochromic detection of chromium with ascorbic acid functionalized luminescent Bio-MOF-1

Gurjeet Kaur[1,2], Saloni Sharma[1,2], Neha Bhardwaj[3], Manoj K Nayak[1,2,*], Akash Deep[1,3,*]

[1]Academy of Scientific and Innovative Research (AcSIR), Ghaziabad- 201002, India; [2]CSIR-Central Scientific Instruments Organization (CSIR-CSIO), Sector 30, Chandigarh-160030, India; [3]Institute of Nano Science and Technology (INST), Sector 81, Mohali, Punjab- 140306, India

Correspondence: manoj.nayak@csio.res.in (MKN), akashdeep@inst.ac.in (AD)

Table S1. Comparison of performance of Bio-MOF-1/AA with other recently reported detection probes for Cr(VI)

Type of sensor	Detection mechanism	Detection limit	Linear range	Ref.
g-C_3N_4 [a]NS	On–Off–On Fluorescence	0.11 μM	0.63-300 μM	[67]
g-C_3N_4/Fe_3O_4 nanocomposites	Fluorescence quenching	0.5 μM	0-600 μM	[26]
[b]AuNPs	Fluorescence quenching	3.3 nM.	0.1–0.8 μM	[68]
[c]CDs	Fluorescence quenching	0.16 μM	0.8 ~ 189 μM	[69]
[d]PANI@Nd-LDH	Fluorescence quenching	1.5 nM	200-1000 ppb	[70]
[e]DECDs	Ratiometric fluorescence	0.4 μM	2-300 μM	[71]
Gold nanoparticles (AuNPs)	Fluorescence quenching	10^{-7} M	10^{-7}-10^{-3} M	[72]
[f]PANI/AgNPs/GO nanocomposite	Luminescence quenching	0.33 nM	0.52-390 nM	[27]
[g]CDs@Eu-MOFs	Ratiometric fluorescence	0.21 μM	2-100 μM	[73]
Bio-MOF-1/AA	Fluorescence enhancement	0.01 ng/mL (0.52 pM)	0.02-20 ng/mL (0.001-1.0 nM)	**This work**

Notes: [a]nanosheets; [b]Gold nanoparticles; [c]Carbon Dots; [d]Neodymium-doped polyaniline Zn-Al layered double hydroxide; [e]Dual emissive carbon dots; [f]Polyaniline/Silver nanoparticles/graphene oxide; [g]carbon dots@Europium metal-organic frameworks

Table S2: Results of the ANOVA test at a 5% significance level for the reproducibility test measurements of Bio-MOF-1-AA chemosensor response

Source	Sum of Squares SS	Degrees of Freedom ν	Mean Square MS	F statistic	p-value
Treatment	4,234.2667	4	1,058.5667	1,221.4231	2.1294e-13
Error	8.6667	10	0.8667		
Total	4,242.9333	14			

Table S3: Results of Tukey's multiple comparisons test on various matching pairs.

Treatments pair	Tukey HSD Q statistic	Tukey HSD p-value	Tukey HSD Inference
Cycle I vs Cycle II	11.1631	0.0010053	p<0.01
Cycle I vs Cycle III	76.2814	0.0010053	p<0.01
Cycle I vs Cycle IV	32.2490	0.0010053	p<0.01
Cycle I vs Cycle V	42.7920	0.0010053	p<0.01
Cycle II vs Cycle III	87.4445	0.0010053	p<0.01
Cycle II vs Cycle IV	43.4122	0.0010053	p<0.01
Cycle II vs Cycle V	53.9551	0.0010053	p<0.01
Cycle III vs Cycle IV	44.0323	0.0010053	p<0.01
Cycle III vs Cycle V	33.4894	0.0010053	p<0.01
Cycle IV vs Cycle V	10.5430	0.0010053	p<0.01

Table S4: Analysis of Cr(VI) in spiked samples of tap water, lake water, and basil leaves with Bio-MOF-1/AA nanoprobe

Sample	Added Cr(VI) (ng/mL)	Cr(VI) as found by Bio-MOF-1/AA nanoprobe (ng/mL)	Cr(VI) concentration as determined by ICP-MS (ng/mL)	% correlation between ICP-MS and Bio-MOF-1/AA values
Tap Water				
1.	6	6.2±0.04	6.8±0.01	104
2.	8	9.0±0.06	9.1±0.13	112
3.	10	9.9±0.02	9.6±0.08	98
Lake Water				
1.	6	6.5±0.02	6.6±0.09	108
2.	8	8.8±0.05	9.1±0.12	110
3.	10	10.3±0.03	10.4±0.07	102
Basil Leaves				
1.	6	6.0±0.01	6.9±0.04	99
2.	8	8.3±0.06	9.0±0.08	104
3.	10	10.1±0.03	9.6±0.02	100

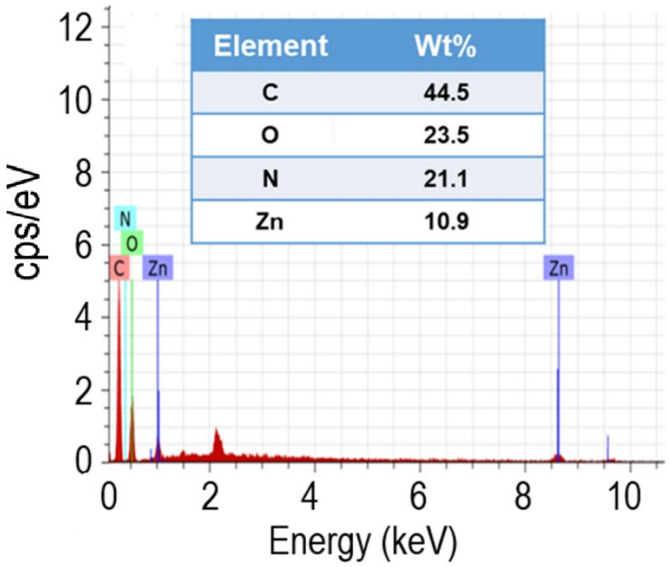

Fig. S1. EDX based elemental composition of Bio-MOF-1

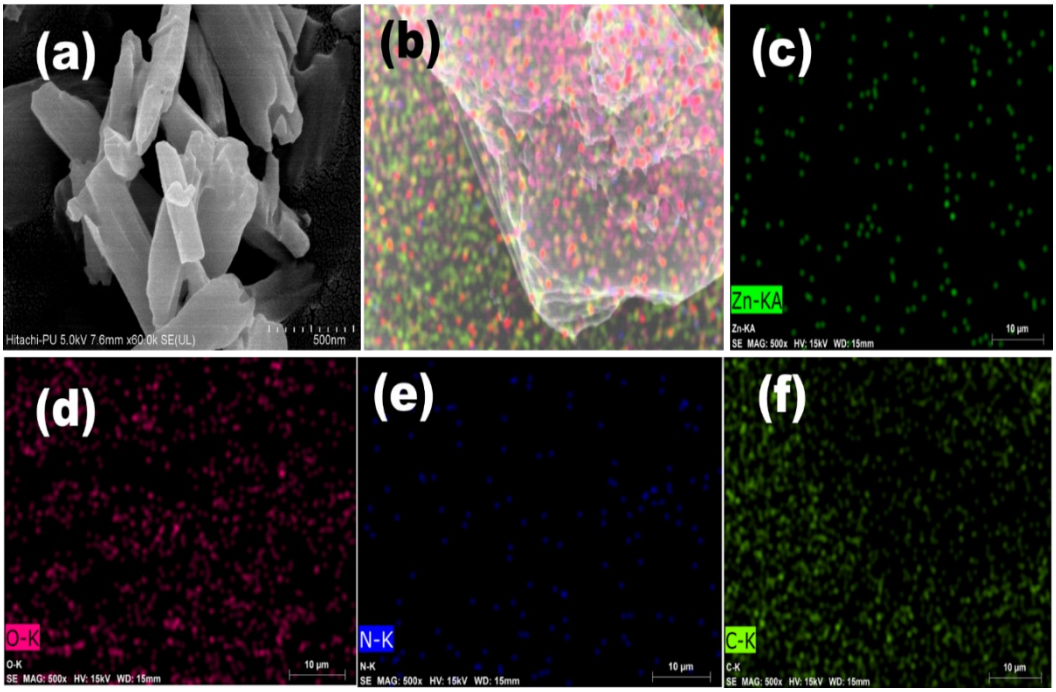

Fig. S2. Elemental mapping images of (a-f): Bio-MOF-1/AA.

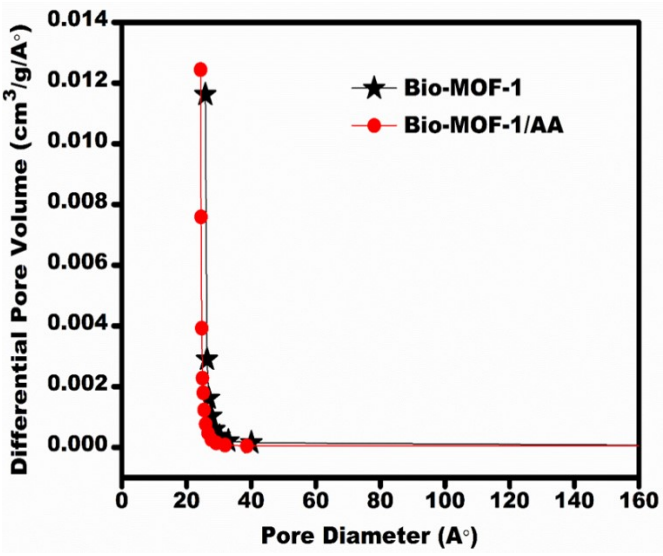

Fig. S3. BJH adsorption pore-size distributions for Bio-MOF-1 and Bio-MOF-1/AA.

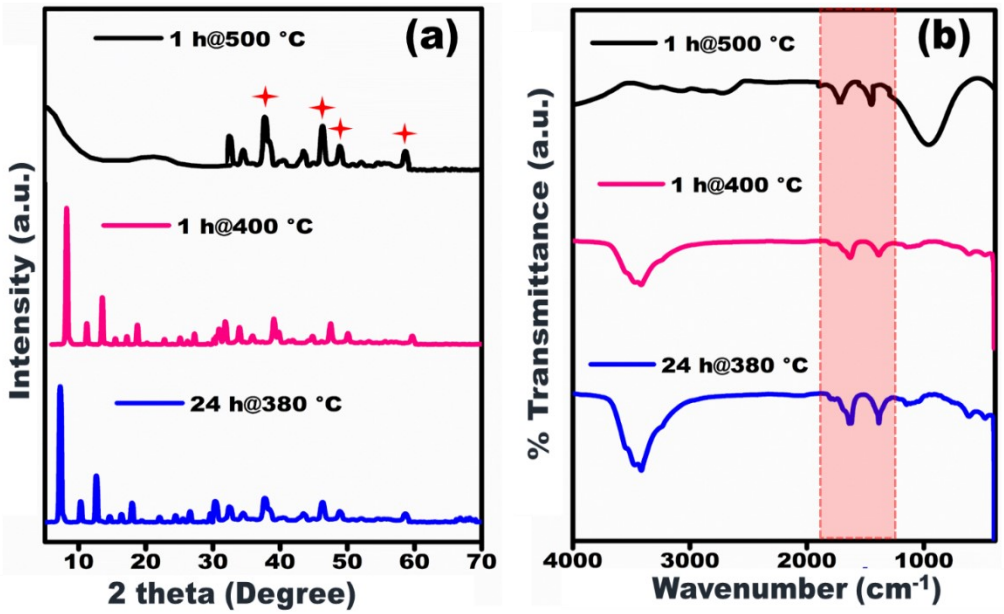

Fig. S4. Structural characterizations of thermally annealed Bio-MOF-1/AA samples at 380, 400 and 500 °C. (a): XRD patterns; the asterisks represent the peaks for ZnO; (b): FTIR spectra show retention of all the framework IR modes.

IR bands in the region (1680−1300) cm^{-1} are assigned to asymmetric and symmetric modes of carboxylates, region (1300–600) cm^{-1} are assigned to the in-plane and out-of-plane deformation modes of the aromatic ring, a band at 480 cm^{-1} is a characteristic Zn–O stretching vibration band of the tetrahedral coordinated Zn_4O cluster and broad band in the region (800−500) cm^{-1} is assigned to the Zn–O stretching in ZnO which is more prominent in the samples annealed at 500 °C. The highlighted regions show changes in carboxylate asymmetric and symmetric vibrations.

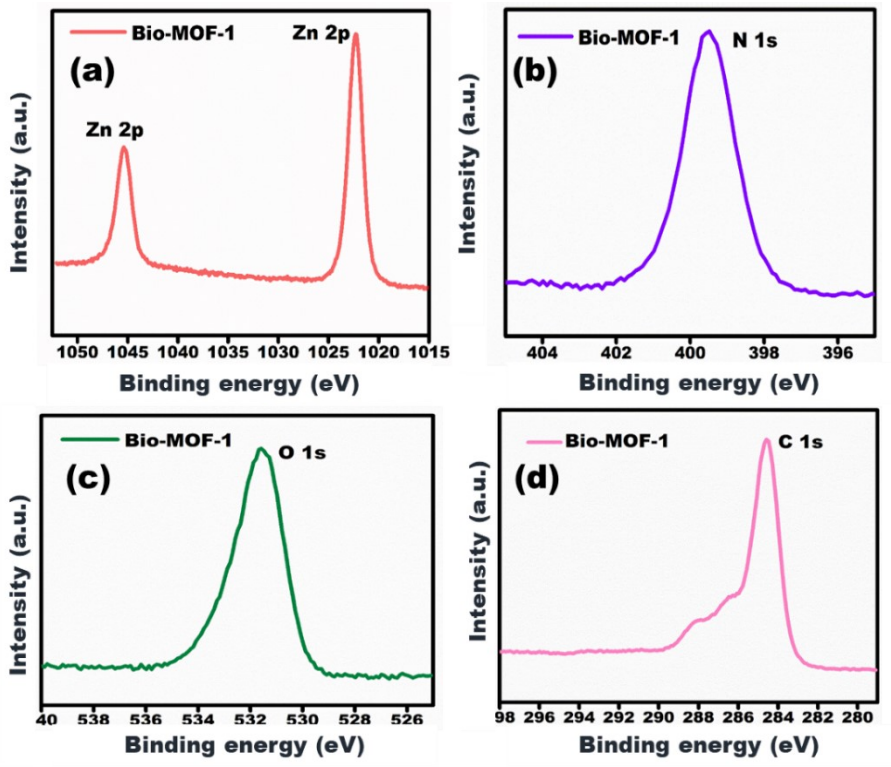

Fig. S5. XPS spectra of Bio-MOF-1. (a): Zn2p; (b): N1s; (c): O1s; (d): C1s

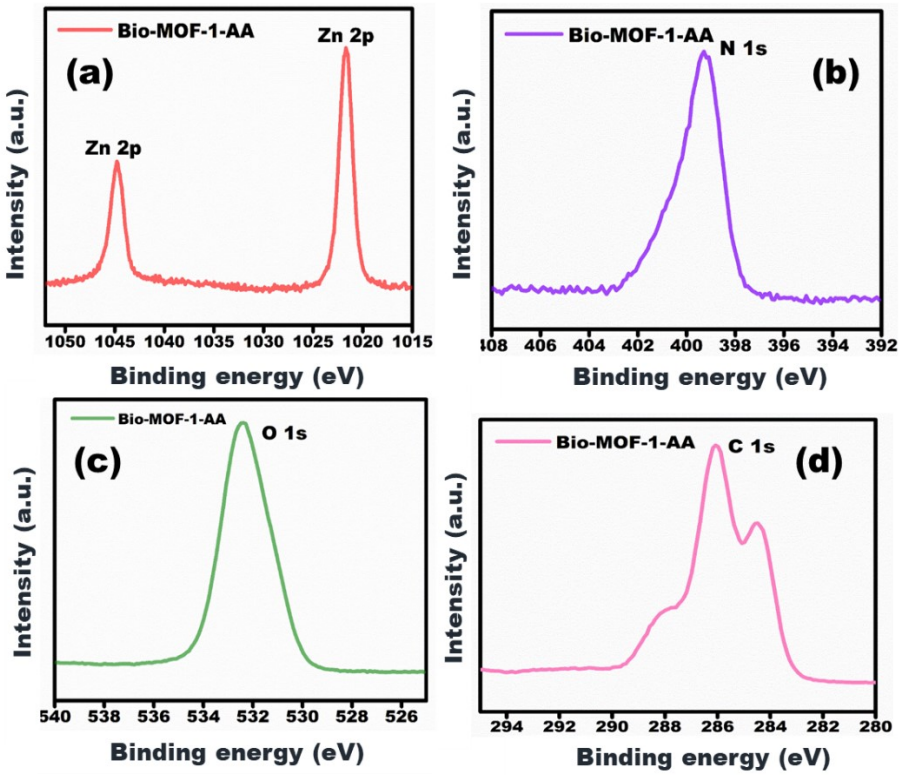

Fig. S6. XPS spectra of Bio-MOF-1/AA (a): Zn2p; (b): N1s; (c): O1s; (d): C1s

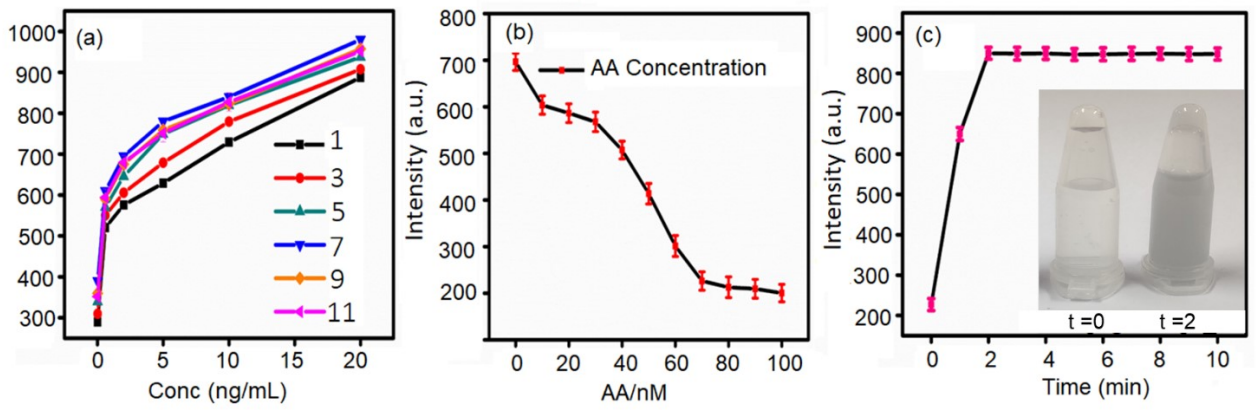

Fig. S7. Optimization of experimental conditions for sensing of Cr(VI) by Bio-MOF-1/AA. (a): Effect of pH of test solution on PL intensity; (b): Effect of concertation of ascorbic acid on PL intensity of formed Bio-MOF-1/AA product. *AA in a concentration of 70 ng/mL allowed the formation of a nanoprobe complex with maximum quenching*; (c): Change in PL intensity at different incubation times upon addition of 100 µL of 0.001 nM Cr(VI). *Inset:(Visual change in colour of nanoprobe solution after 2 min upon addition of 100 µL of 0.001 nM Cr(VI).*

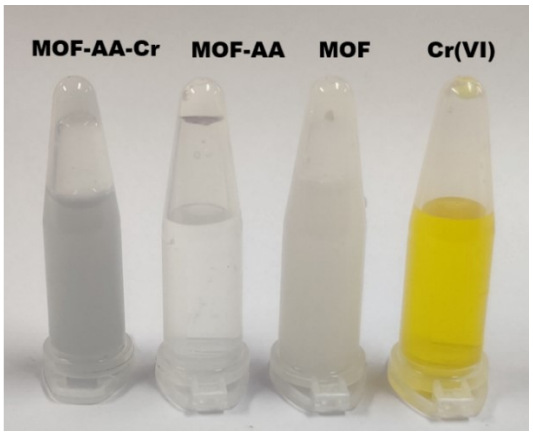

Fig. S8. Visual development of color as Cr(VI) is added in to Bio-MOF-1/AA solution.

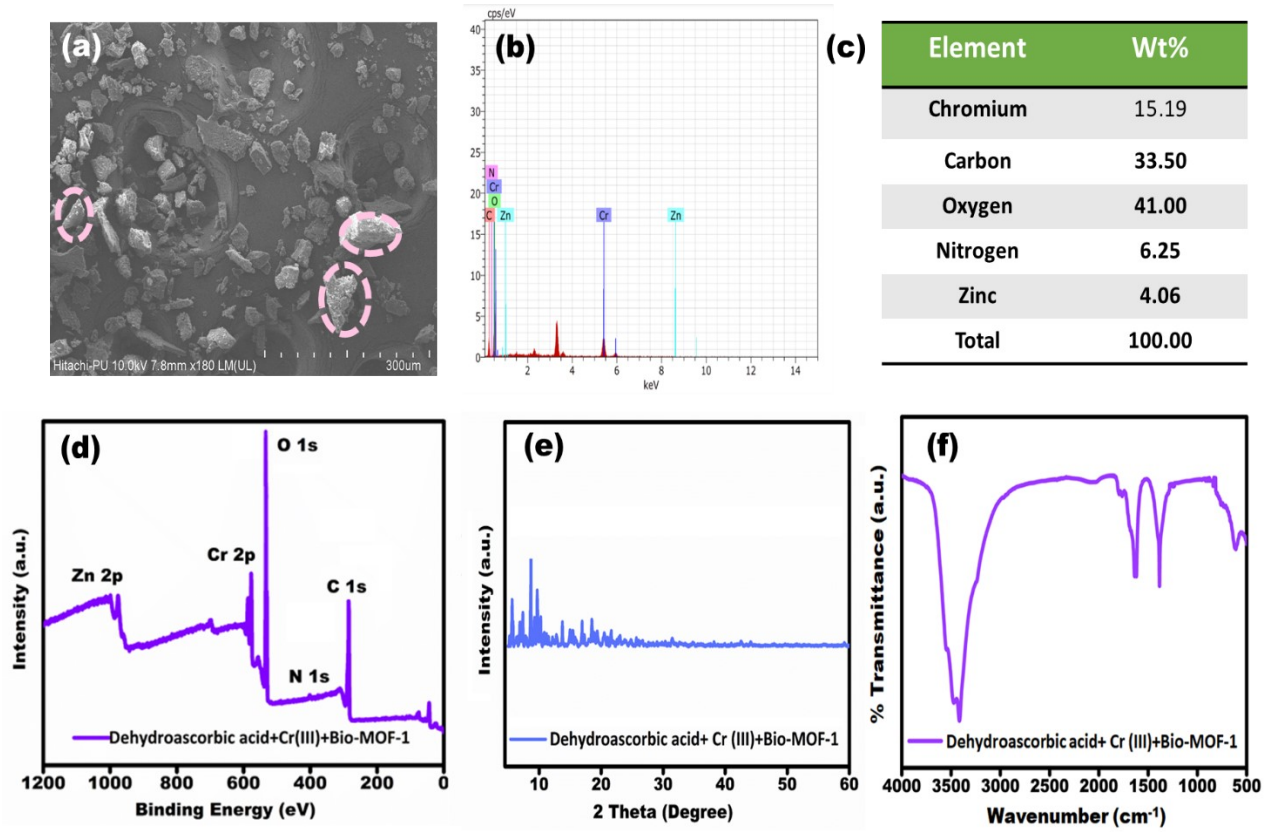

Element	Wt%
Chromium	15.19
Carbon	33.50
Oxygen	41.00
Nitrogen	6.25
Zinc	4.06
Total	100.00

Fig. S9. Characterization of reaction product formed between Bio-MOF-1/AA and Cr(VI), i.e. DHA+Cr(III) and Bio-MOF-1. (a): SEM image, *encircled structures refer to DHA+Cr(III) aggregates*; (b-c): EDX analysis and elemental composition; (d): XPS spectrum; (e): XRD patterns; (f): FTIR spectrum

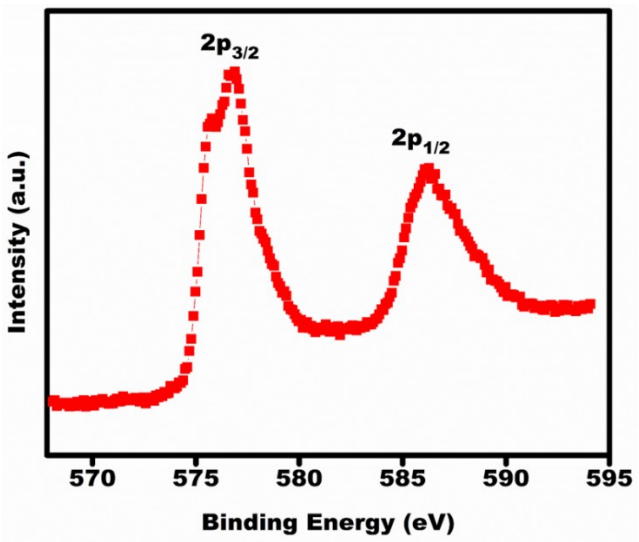

Fig. S10. High-resolution XPS spectra ($2p_{3/2}$ and $2p_{1/2}$ regions) of reaction product formed between Bio-MOF-1/AA and Cr(VI)

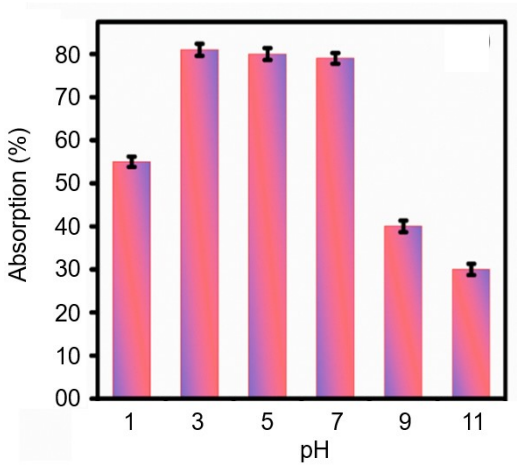

Fig. S11. Dependence of pH on the adsorption of Cr(VI) (1 µg/mL) with Bio-MOF-1/AA complex (1 mg/mL), *Time of incubation = 5 min*